Electrophoresis of a Finite Cylinder along the Axis of a Cylindrical Pore

Jyh-Ping Hsu* and Chen-Yuan Kao

Department of Chemical Engineering, National Taiwan University, Taipei, Taiwan 10617, R.O.C.

Received: April 5, 2002

The boundary effect on the electrophoresis of an entity is of both fundamental and practical significance. Typical examples include the electrophoresis in a narrow space such as a pore and that of a concentrated dispersion. In this study, the boundary effect on the electrophoretic behavior of a particle is investigated theoretically by considering a finite, charged, cylindrical particle in an uncharged cylindrical pore for the case of low electrical potential. We show that while the direction of the movement of a particle is determined by the charged conditions on its lateral surface, the magnitude of its mobility is mainly controlled by that of the top and bottom surfaces of the particle. It is interesting to note that the mobility of a uniformly charged particle may have a local maximum as the ratio (particle radius/pore radius) varies. The mobility decreases with the increase in the aspect ratio (particle radius/particle length) of the particle. The effect of the presence of the pore on the electrophoretic mobility of the particle increases significantly as the charge density on particle surface increases.

I. Introduction

Electrophoresis is one of the most widely adopted analytical tools in the study of the surface properties of colloidal particles. It also plays an important role in both biochemistry and biophysics when purification and characterization of biochemical materials are involved. Apparently, a detailed understanding of the electrophoretic behavior of a colloidal particle is essential to both fundamental theory and applications. The analysis of this problem, however, is not an easy task. This is mainly due to the complicated interaction between hydrodynamic and electric effects, and the governing equations involved are coupled nonlinear differential equations. Smoluchowski[1] derived the following relation between the electrophoretic velocity $\boldsymbol{U}$ of an isolated, nonconducting, charged particle in an infinite electrolyte solution of viscosity η and permittivity ϵ and an applied field $\boldsymbol{E}$:

$$\boldsymbol{U} = \frac{\epsilon\zeta\boldsymbol{E}}{\eta} \tag{1}$$

where ζ is the zeta potential of the particle. This expression is applicable to a particle of arbitrary shape, provided that its local radius of curvature is much larger than thethickness of the double layer surrounding it.[2] The ratio $\boldsymbol{U}/\boldsymbol{E}$ is known as the electrophoretic mobility of the particle.

In many applications of electrophoresis, colloidal particles are not isolated, and they move under the influence of neighboring particles or the presence of boundaries. A typical example of the former includes the electrophoresis of a concentrated dispersion where the interaction between neighboring particles is significant, and that for the latter includes the electrophoresis through a pore in a membrane which occurs in electrophoretic separation of proteins. Modification of the Smoluchowski equation to take these effects into account is necessary from a practical point of view. Relevant studies are ample in the literature. Most of them, however, are based on entities of one-dimensional nature such as spheres[3−22] and infinite cylinders.[23−28] Note that in the latter the end effect of a particle is neglected. For particles of other shapes,[29−34] the electrokinetic calculations are usually complicated and time-consuming, and therefore, most of the relevant works are based on the assumption of a thin double layer.[4−11,13,15,16,26,27,29,30,32,33] In this case, the solution procedure for the electric field can be simplified dramatically. In practice, colloidal particles can assume arbitrary geometry,[1] and extension of previous analyses to a more general case is highly desirable. Another important factor is the nonhomogeneous nature of the charged conditions on the particle surface. The charge on the basal plane of a kaolin particle, for instance, can have a different sign than that on its facial plane. Including this effect in the relevant analysis seems to be realistic.

In this study we consider the electrophoresis of a finite, nonuniformly charged, nonconducting cylindrical particle with a moderately thick electrical double layer. Several specific shapes can be simulated by adjusting the aspect ratio of the particle. For example, it may represent a plate-like particle such as montmorillonite with a nonuniform surface charge distribution. The boundary effects are also examined by considering the case where the particle is moving along the axis of cylindrical pore.

II. Theory

The space charge density of an electrolyte solution containing an ionic species of number density n_i and valence z_i is

$$\rho = \sum_i ez_i n_i \tag{2}$$

where e is the elementary charge. Suppose that the electrical potential Ψ can be described by Poisson's equation,

$$\nabla^2\Psi = -\frac{\rho}{\epsilon} \tag{3}$$

* Corresponding author. Fax: 886-2-23623040. E-mail: jphsu@ccms.ntu.edu.tw

10.1021/jp0209087 CCC: $22.00
Published on Web 09/24/2002

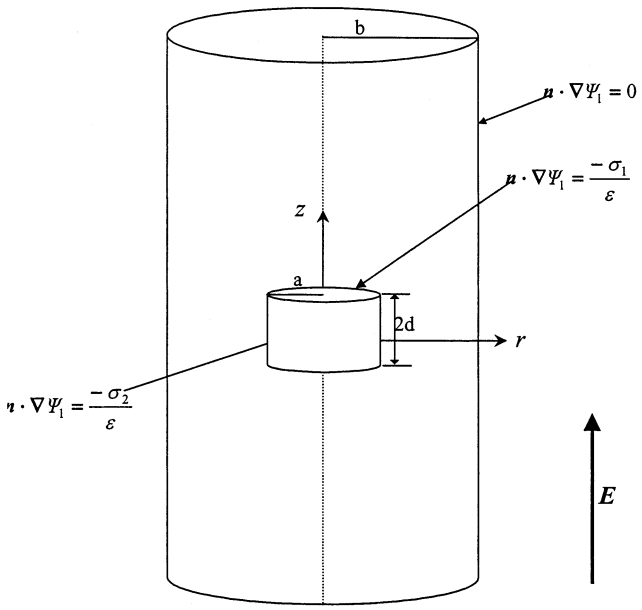

Figure 1. Schematic representation of the problem considered. A charged cylindrical particle of radius a and length $2d$ is placed on the axis of an uncharged, infinite cylindrical pore of radius b. An electric field $\boldsymbol{E}$ parallel to the axis of the pore is applied. σ_1 is the charge density on the top and bottom surfaces of the particle, and σ_2 is that on the lateral surface.

where ϵ is the permittivity of the electrolyte solution. At steady state, the distribution of the ions can be described by the conservation equation,

$$\nabla\left[n_i\boldsymbol{u} - D_i\left(\nabla n_i + \frac{ez_i n_i}{k_B T}\nabla\Psi\right)\right] = 0 \tag{4}$$

where ∇ is the gradient operator, D_i is the diffusivity of ions of species i, k_B is the Boltzmann constant, T is the absolute temperature, and $\boldsymbol{u}$ is the fluid velocity. We assume that the flow field can be described by the Navier−Stokes equation in the creeping flow regime

$$\eta\nabla^2\boldsymbol{u} - \nabla p = \rho\nabla\Psi \tag{5}$$

$$\nabla\bullet\nabla\boldsymbol{u} = 0 \tag{6}$$

where η is the fluid viscosity and p is the pressure. The term on the right-hand side of eq 5 denotes the electrical body force. For simplicity, we consider an incompressible fluid with constant physical properties.

Referring to Figure 1, we consider a rigid, nonconducting, cylindrical particle of radius a and length $2d$ on the axis of an infinite cylindrical pore of radius b filled with an electrolyte solution. Because the length of the particle is comparable to its radius, the end effect of the top and bottom surfaces of the particle can be significant. A uniform electric field $\boldsymbol{E}$ in the direction along the axis of the cylindrical pore is applied, and the particle moves along the axis of the pore; that is, an axisymmetric problem is considered. Let σ_1 be the charge density on the top and bottom surfaces of the particle and σ_2 be that on the lateral surface. The cylindrical coordinates are chosen with its origin located at the center of the particle. The axisymmetric nature of the geometry adopted suggests that only the (r,z) domain needs to be considered.

2.1. Electrical Field. Following Henry's[35] classic treatment, we assume that the electrical potential Ψ can be expressed as a linear superposition of the electrical potential in the absence of the applied electric field (i.e., equilibrium potential), Ψ_1, and the electrical potential outside the particle that arises from the applied field, Ψ_2. This assumption is valid under conditions where the applied electric field is weak relative to the electric fields induced by the particle. This implies that the ionic cloud surrounding the particle is only slightly distorted by the applied electric field; that is, the effect of double layer polarization is negligible. Therefore, the ionic concentrations can be assumed to attain their equilibrium distributions, which can be obtained from eq 4 by letting $\boldsymbol{u} = 0$. It can be shown that

$$n_i = n_{i0}\exp\left(\frac{-ez_i\Psi_1}{k_B T}\right) \tag{7}$$

where n_{i0} is the bulk number density of ionic species i. If the electrical potential is low, the Debye−Hückel approximation is applicable and Ψ_1 can be described by

$$\nabla^2\Psi_1 = \kappa^2\Psi_1 \tag{8}$$

where the inverse Debye length or Debye−Hückel parameter κ is defined by

$$\kappa = \left(\frac{e^2\sum_i z_i^2 n_{i0}}{\epsilon k_B T}\right)^{1/2} \tag{9}$$

Similarly, the electrical potential associated with the applied electric field Ψ_2 can be described by

$$\nabla^2\Psi_2 = 0 \tag{10}$$

The boundary conditions associated with eqs 8 and 10 are assumed as

$$\boldsymbol{n}\bullet\nabla\Psi_1 = \frac{-\sigma_1}{\epsilon}, \frac{\partial\Psi_2}{\partial z} = 0, |z| = d, 0 \le r \le a \tag{11}$$

$$\boldsymbol{n}\bullet\nabla\Psi_1 = \frac{-\sigma_2}{\epsilon}, \frac{\partial\Psi_2}{\partial r} = 0, r = a, -d \le z \le d \tag{12}$$

$$\boldsymbol{n}\bullet\nabla\Psi_1 = 0, \frac{\partial\Psi_2}{\partial r} = 0, r = b \tag{13}$$

$$\Psi_1 = 0, \nabla\Psi_2 = -\boldsymbol{E}, |z| \to \infty, r < b \tag{14}$$

In these expressions $\boldsymbol{n}$ is the unit normal directed into the liquid phase.

2.2. Flow Field. The axisymmetric nature of the problem under consideration and the charged conditions on the particle surface imply that it will move in the direction of the applied electric field; the particle moves in the direction of the applied electric field and the torque it experienced vanishes. Following the treatment of Ennis and Anderson[17] or Shugai and Carnie,[20] the governing equations for the electric field and the flow field are decoupled by expanding each dependent variable in a double perturbation series in E and ζ, and neglecting all the nonlinear terms.[17,20] Equations 5 and 6 become, after the expansion treatment,

$$\eta\nabla^2\boldsymbol{u}^{(1,1)} - \nabla p^{(1,1)} = \rho^{(0,1)}\nabla\Psi^{(1,0)} \tag{15}$$

$$\nabla\bullet\nabla\boldsymbol{u}^{(1,1)} = 0 \tag{16}$$

where $\rho^{(0,1)} = -\epsilon\kappa^2\Psi_1$, $\Psi^{(1,0)} = \Psi_2$, and the superscripts denote

the order in (E,ξ) of the quantity. The boundary conditions associated with these equations are assumed as

$$\boldsymbol{u} = U\boldsymbol{i}_z \text{ on particle surface} \tag{17}$$

$$\boldsymbol{u} = 0,\ r = b \tag{18}$$

$$\boldsymbol{u} = 0,\ |z| \rightarrow \infty,\ r < b \tag{19}$$

where $\boldsymbol{i}_z$ is the unit vector in the z-direction. Equations 17 and 18 arise from the no-slip condition on both the particle surface and the pore wall.

2.3. Electrophoretic Mobility. The total force acting on the particle comprises the hydrodynamic force and the electrostatic force. The axisymmetric nature of the problem under consideration suggests that only the forces in the z-direction need to be evaluated. The electrostatic force experienced by the particle in the z-direction can be calculated by

$$F_E^Z = \int\int_S \sigma^{(0,1)} E_Z^{(1,0)}\, \mathrm{d}S = \int\int_S \sigma^{(0,1)} \left(-\frac{\partial \Psi^{(1,0)}}{\partial z}\right) \mathrm{d}S \tag{20}$$

where S denotes the surface of the particle. The hydrodynamic force acting on the particle in the z-direction, F_D^Z, can be decomposed into two terms: one that arises from the viscous force, F_{DV}^Z, and one that arises from the hydrodynamic pressure, F_{DP}^Z; that is,

$$F_D^Z = F_{DV}^Z + F_{DP}^Z \tag{21}$$

F_{DV}^Z and F_{DP}^Z can be calculated respectively by

$$F_{DV}^Z = \int\int_S \eta \frac{\partial(\boldsymbol{u}\bullet\boldsymbol{t})}{\partial n} t_z\, \mathrm{d}S \tag{22}$$

$$F_{DP}^Z = \int\int_S -pn_z\, \mathrm{d}S \tag{23}$$

where $\boldsymbol{t}$ is the tangential unit vector on the particle surface, and t_z and n_z are respectively the z-component of $\boldsymbol{t}$ and $\boldsymbol{n}$. The mobility of the particle can be calculated based on the fact that the total force acting on it vanishes at steady state; that is,

$$F_D^Z + F_E^Z = 0 \tag{24}$$

III. Results and Discussion

The behavior of the system under consideration is examined through numerical simulation. The governing equations and the associated boundary conditions are solved by FlexPDE,[36] a partial differential solver based on a finite element method, on an IBM-PC compatible machine. The solution procedure is summarized in the following steps. (Step 1) Solve eqs 8 and 10 subject to boundary conditions, eqs 11−14, for the electric potentials Ψ_1 and Ψ_2, and calculate the electrostatic force F_E^Z by eq 20. (Step 2) Substitute Ψ_1 and Ψ_2 into eq 15 and solve the resultant equation simultaneously with eq 16,[37] using an initially guessed velocity $\boldsymbol{U}$ to evaluate $\boldsymbol{u}$ and p. The hydrodynamic forces F_{DV}^Z and F_{DP}^Z are then calculated by eqs 22 and 23. If eq 24 is satisfied, then the solution procedure is completed. Otherwise, go to the next step. (Step 3) A new value for $\boldsymbol{U}$ is assumed back to step 2. In step 2, the criterion $|(F_E^Z + F_D^Z)/F_E^Z| \leq 0.5\%$ is adopted to determine if eq 24 is satisfied. For convenience, a dimensionless electrophoretic mobility μ^* defined below is used in subsequent discussions:

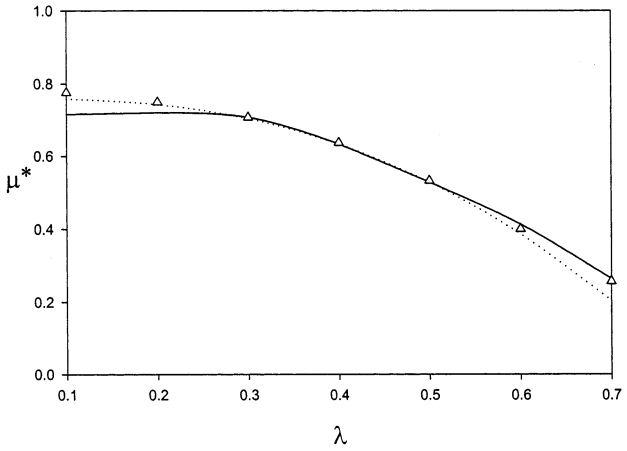

Figure 2. Variation of scaled mobility μ^* ($= \boldsymbol{U}\eta/\zeta_S\boldsymbol{E}\epsilon$) as a function of λ for the case where a sphere of constant surface potential ζ_S is placed on the axis of an uncharged cylindrical pore. Parameters used are $\kappa a = 4.3$, $\zeta_S = k_B T/e$. Δ is the numerical result based on FlexPDE, the dashed line represents results based on the reflection method of Ennis and Anderson,[17] and the solid line is the numerical result of Shugai and Carnie.[20]

$$\mu^* = \frac{\boldsymbol{U}\eta}{\zeta_{\mathrm{REF}}\boldsymbol{E}\epsilon} \tag{25}$$

where $\zeta_{\mathrm{REF}} = k_B T/e$ is a reference potential. The applicability and accuracy of the software used are checked by comparing with the available results in the literature. Because we cannot find a system that matches exactly with our problem, the results for the electrophoresis of a sphere along the axis of a cylindrical pore examined by Ennis and Anderson[17] and Shugai and Carnie[20] are adopted.[17,20] The former solved the problem based on a reflection method, and the latter solved it numerically. Figure 2 shows the results based on these approaches and that based on our approach. Shugai and Carnie[20] concluded that, due to numerical error, their numerical approach was inappropriate for small λ (ratio of particle radius to pore radius). On the other hand, due to the overlap of double layers, the reflection method might not provide accurate results if λ is large. Figure 2 reveals that our approach does not have these limitations, and it seems to work well for the range of λ considered.

Figure 3 shows the variation of the scaled electrophoretic mobility μ^* as a function of λ ($= a/b$) for various particle aspect ratios a/d and κa. Here, the surface of the particle is uniformly charged. Figure 3 reveals that the smaller the μ^* (thicker double layer) the smaller the μ^*. This is because if the double layer is thick, the influence of the electric body force is capable of reaching a deep region in the liquid phase. Figure 3 also indicates that $\mu^* \rightarrow 0$ as $\lambda \rightarrow 1$. This is expected because $\lambda \rightarrow 1$ implies that the particle attaches the wall of the pore. The trend that μ^* decreases with the increase in λ shown in Figure 3 is similar to that for the case of a sphere in a cylindrical pore.[17,20] It is interesting to note, however, that if a/d is large, μ^* may exhibit a local maximum as λ varies, which is not observed for the corresponding sphere-in-cylinder problem.

The variations of the scaled electrophoretic mobility μ^* as a function of λ for various particle aspect shapes a/d and κa are illustrated in Figure 4. Here, the surface of the particle is nonuniformly charged. As can be seen from Figure 4, μ^* increases with the increase in κa, but decreases with the increase

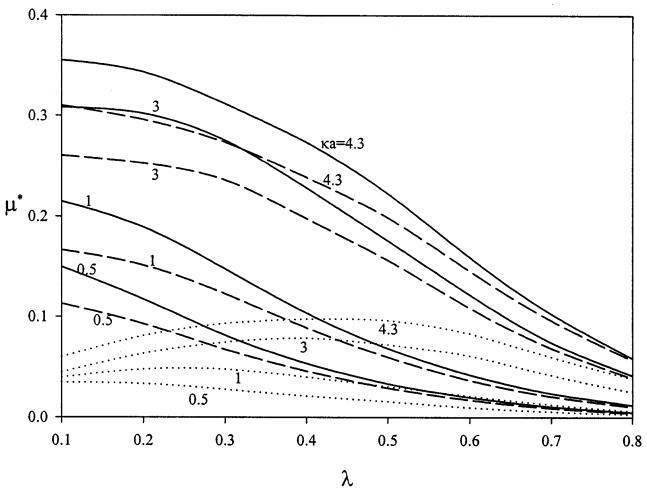

Figure 3. Variation of scaled electrophoretic mobility μ^* ($=\boldsymbol{U}\eta/\zeta_{REF}\boldsymbol{E}\epsilon$) as a function of λ ($=a/b$) at various particle aspect ration a/d and κa. Parameters used are $\sigma_1 = \sigma_2 = 0.5$ ($\epsilon\kappa k_B T/e$), $\zeta_{REF} = k_B T/e$. Solid lines, $a/d = 1/2$, dashed lines, $a/d = 1$, dotted lines, $a/d = 8$.

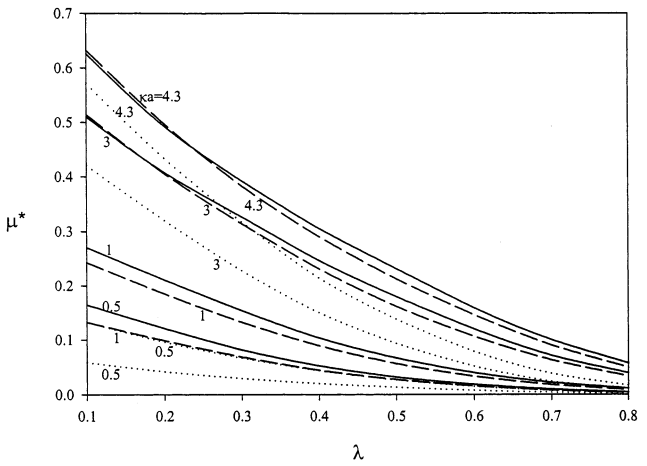

Figure 4. Variation of scaled electrophoretic mobility μ^* as a function of λ for the case of Figure 3 at various particle aspect ratios a/d and κa. Parameters used are the same as Figure 3, except that $-\sigma_1 = \sigma_2 = 0.5$ ($\epsilon\kappa k_B T/e$). Solid lines, $a/d = 1/2$, dashed lines, $a/d = 1$, dotted lines, $a/d = 8$.

in λ, as expected. Note that the local maximum of μ^* as λ varies shown in Figure 3 does not appear in the present nonuniformly charged condition. This implies that the direction of the translational motion of a particle is dominated by the sign of the charge on its lateral surface: if $\sigma_2 > 0$, the particle moves in the direction of the applied electric field, and the reverse is true if $\sigma_2 < 0$. On the other hand, the magnitude of the mobility of a particle is influenced mainly by the sign of the charge on its top and bottom surface.

Figure 5 shows the variation of the scaled electrophoretic mobility μ^* as a function of λ for the case of Figure 3. It reveals that the larger the a/d, the smaller the scaled electrical mobility μ^*. Figure 5 indicates that as a/d increases, the value of λ at which the local maximum of μ^* occurs shifts to a larger value, and the shape of the μ^* against λ curve becomes flatter. Also, the larger the κa, the smaller the value of a/d needed to observe the local maximum in μ^*. Figure 5 also suggests that for fixed κa, while the difference in the μ^* between various particle aspect ratios is appreciable as $\lambda \rightarrow 0$, it becomes inappreciable as $\lambda \rightarrow 1$. That is, the effect of boundary (pore wall) on the electrophoretic behavior of a particle depends on its shape; the closer

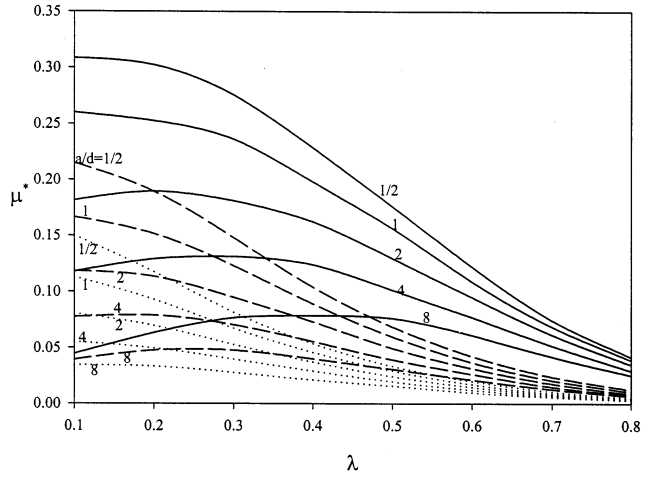

Figure 5. Variation of scaled electrophoretic mobility μ^* as a function of λ for the case of Figure 3 for various particle aspect ratios (a/d) at various particle aspect ratios a/d. Solid lines, $\kappa a = 3$, dashed lines, $\kappa a = 1$, dotted lines, $\kappa a = 0.5$.

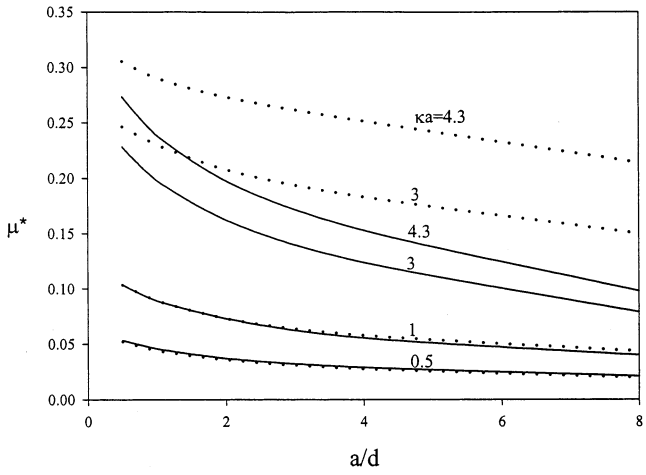

Figure 6. Variation of scaled electrophoretic mobility μ^* as a function of particle aspect ratio a/d for the case of Figures 3 or 4 with $\lambda = 0.4$ for different surface charge density at various κa. Solid lines, $\sigma_1 = \sigma_2 = 0.5(\epsilon\kappa k_B T/e)$, dashed lines, $-\sigma_1 = \sigma_2 = 0.5(\epsilon\kappa k_B T/e)$.

the particle radius to pore radius, the less the difference between the behaviors of particles of different shapes.

Figure 6 shows the variation of the scaled electrophoretic mobility μ^* as a function of its aspect ratio a/d for various κa at two different charged conditions on the particle surface. This figure indicates that, for a fixed κa, μ^* decreases with the increase in a/d, in general. Note that, if κa is small, the effect of the charged conditions on particle surface on μ^* is insignificant. However, if κa is large, μ^* becomes sensitive to the charged conditions on the particle surface. In this case, the mobility of a particle with its lateral surface and top and bottom surfaces carrying different charges is greater than the mobility of a uniformly charged particle. Note that as $a/d \rightarrow 0$ (i.e., infinitely long particle), the effect of the charged conditions on particle surface on μ^* becomes insignificant again.

Figure 7 shows the variation of the scaled electrophoretic mobility μ^* as a function of λ for various types of charged conditions and particle aspect ratios a/d. This figure reveals that μ^* increases with the increase in the charge density on particle surface, as expected. According to Figure 7, it seems that the occurrence of the local maximum in μ^* as λ varies is independent of the level of the charge density on a particle; it

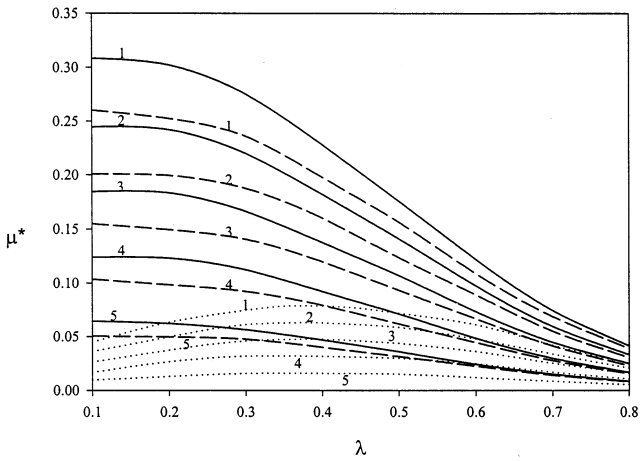

Figure 7. Variation of scaled electrophoretic mobility μ^* as a function of λ at various surface charge density and particle aspect ratios a/d for the case of Figure 3. Parameters used are $\kappa a = 3$, $\zeta_{REF} = k_BT/e$. Solid lines, $a/d = 1/2$; dashed lines, $a/d = 1$; dotted lines, $a/d = 8$. Curve 1, $\sigma_1 = \sigma_2 = 0.5(\epsilon\kappa k_BT/e)$. Curve 2, $\sigma_1 = \sigma_2 = 0.4(\epsilon\kappa k_BT/e)$. Curve 3, $\sigma_1 = \sigma_2 = 0.3(\epsilon\kappa k_BT/e)$. Curve 4, $\sigma_1 = \sigma_2 = 0.2$ $(\epsilon\kappa k_BT/e)$. Curve 5, $\sigma_1 = \sigma_2 = 0.1$ $(\epsilon\kappa k_BT/e)$.

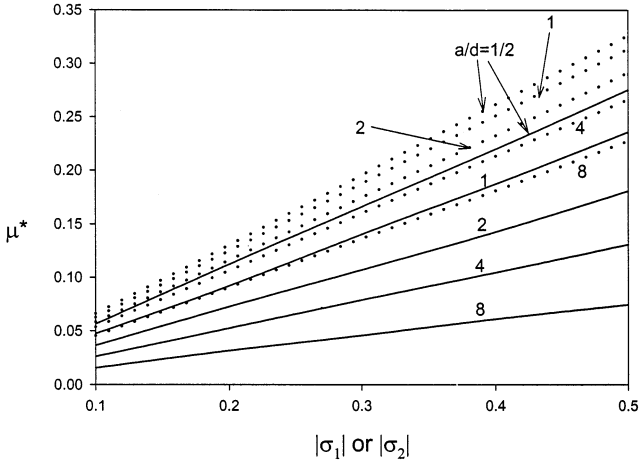

Figure 8. Variation of scaled electrophoretic mobility μ^* as a function of surface charge density $|\sigma_1|$ (or $|\sigma_2|$) for the case of Figure 3 at two different surface charge densities for various particle aspect ratios a/d for the case $\lambda = 0.3$ and $\kappa a = 3$. Solid lines, $\sigma_1 = \sigma_2 = 0.5(\epsilon\kappa k_BT/e)$; dashed lines, $-\sigma_1 = \sigma_2 = 0.5(\epsilon\kappa k_BT/e)$.

depends largely on its shape. Figure 7 also suggests that the lower the charge density, the less sensitive the variation of μ^* as λ varies.

Figure 8 illustrates the variation of the scaled electrophoretic mobility μ^* as a function of its surface charge density for the case of Figure 3 at various particle aspect ratios a/d at two different charged conditions on the particle surface. For illustration, we assume $|\sigma_1| = |\sigma_2|$. Figure 8 reveals that the mobility of a particle is (roughly) positively linearly dependent on its surface charge density. Also, the mobility of a particle with its lateral surface and top and bottom surfaces oppositely charged is greater than the mobility of a uniformly charged particle. This is consistent with the results shown in Figure 6.

IV. Conclusion

In summary, the electrophoretic behavior of a finite, charged, cylindrical particle along the axis of an uncharged cylindrical pore is studied theoretically. In particular, the effects of the particle aspect ratio (or shape), the charged conditions on its surface, and the thickness of the double layer are examined. We conclude that the direction of the movement of a particle is controlled mainly by the charge on its lateral surface, and the effect of boundary (pore wall) on the mobility of the particle is dominated by the charge on its top and bottom surfaces. The mobility of a uniformly charged particle may have a local maximum as its aspect ratio (particle radius/pore radius) varies.

Acknowledgment. This work is supported by the National Science Council of the Republic of China.

References and Notes

(1) Hunter, R. J. *Foundations of Colloid Science*;Clarendon Press: Oxford, ; Vol. I.
(2) Morrison, F. A. *J. Colloid Interface Sci.* **1970**, *34*, 210.
(3) O'Brien, R. W.; White, L. R. *J. Chem. Soc., Faraday Trans. 2* **1978**, *74*, 1607.
(4) O'Brien, R. W.; Hunter, R. J. *Can. J. Chem.* **1981**, *59*, 1878.
(5) Ohshima, H.; Healy, T. W.; White, L. R. *J. Chem. Soc., Faraday Trans. 2* **1983**, *79*, 1613.
(6) O'Brien, R. W. *J. Colloid Interface Sci.* **1983**, *92*, 204.
(7) Keh, H. J.; Anderson, J. L. *J. Fluid Mech.* **1985**, *153*, 417.
(8) Anderson, J. L. *J. Colloid Interface Sci.* **1985**, *105*, 45.
(9) Keh, H. J.; Chen, S. B. *J. Fluid Mech.* **1988**, *194*, 377.
(10) Keh, H. J.; Lien, L. C. *J. Chin. Inst. Chem. Eng.* **1989**, *20*, 283.
(11) Keh, H. J.; Lien, L. C. *J. Fluid Mech.* **1991**, *224*, 305.
(12) Yoon, B. J. *J. Colloid Interface Sci.* **1991**, *142*, 575.
(13) Solomentsev, Y. E.; Pawav, Y.; Anderson, J. L. *J. Colloid Interface Sci.* **1993**, *158*, 1.
(14) Zydney, A. L. *J. Colloid Interface Sci.* **1995**, *169*, 476.
(15) Keh, H. J.; Chiou, J. Y. *AIChE J.* **1996**, *42*, 1397.
(16) Keh, H. J.; Jan, J. S. *J. Colloid Interface Sci.* **1996**, *183*, 458.
(17) Ennis, J.; Anderson, J. L. *J. Colloid Interface Sci.* **1997**, *185*, 497.
(18) Lee, E.; Chu, J. W.; Hsu, J. P. *J. Colloid Interface Sci.* **1997**, *196*, 316.
(19) Lee, E.; Chu, J. W.; Hsu, J. P. *J. Colloid Interface Sci.* **1998**, *205*, 65.
(20) Shugai, A. A.; Carnie, S. L. *J. Colloid Interface Sci.* **1999**, *213*, 298.
(21) Ohshima, H. *J. Colloid Interface Sci.* **2001**, *239*, 587.
(22) Chu, J. W.; Lin, W. H.; Lee, E.; Hsu, J. P. *Langmuir* **2001**, *17*, 6289.
(23) Stigter, D. *J. Phys. Chem.* **1978**, *82*, 1417.
(24) Stigter, D. *J. Phys. Chem.* **1978**, *82*, 1424.
(25) Sherwood, J. D. *J. Chem. Soc., Faraday Trans. 2* **1982**, *78*, 1091.
(26) Keh, H. J.; Horng, K. D.; Kuo, J. *J. Fluid Mech.* **1991**, *231*, 211.
(27) Keh, H. J.; Chen, S. B. *Langmuir* **1993**, *9*, 1142.
(28) Chen, S. B.; Koch, D. L. *J. Colloid Interface Sci.* **1996**, *180*, 466.
(29) O'Brien, R. W.; Ward, D. N. *J. Colloid Interface Sci.* **1988**, *121*, 402.
(30) Fair, M. C.; Anderson, J. L. *J. Colloid Interface Sci.* **1989**, *127*, 388.
(31) Yoon, B. J.; Kim, S. *J. Colloid Interface Sci.* **1989**, *128*, 275.
(32) Keh, H. J.; Huang, T. Y. *J. Colloid Interface Sci.* **1993**, *160*, 354.
(33) Feng, J. J.; Wu, W. Y. *J. Fluid Mech.* **1994**, *264*, 41.
(34) Sherwood, J. D.; Stone, H. A. *Phys. Fluids* **1995**, *7*, 697.
(35) Henry, D. C. *Proc. R. Soc. A* **1931**, *133*, 106.
(36) FlexPDE version 2.22, PDE Solutions Inc., Scranton, PA.
(37) Backstrom, G. *Fluid Dynamics by Finite Element Analysis*; Studentlitteratur: Sweden, 1999.